Journal of
Nanoscience and Nanotechnology
Vol. 10, 7025–7030, 2010

Nano-Sized $SnSbAg_x$ Alloy Anodes Prepared by Reductive Co-Precipitation Method Used as Lithium-Ion Battery Materials

Mingshu Zhao[1,*], Qingyang Zheng[2], Fei Wang[1], Yufeng Qin[1], and Xiaoping Song[1]

[1] *MOE Key Laboratory for Nonequilibrium Synthesis and Modulation of Condensed Matter, School of Science, Xi'an Jiaotong University, 710049, Xi'an, China*
[2] *Xi'an High-Tech Research Institute, 710025, Xi'an, China*

Nano-sized $SnSbAg_x$ alloy anode materials are prepared by reductive co-precipitation method combining with the aging treatment in water bath at 80 °C. The microstructure, morphology and electrochemical properties of synthesized $SnSbAg_x$ alloy powders are evaluated by X-ray diffraction (XRD), field-emission scanning electron microscopy (FE-SEM), galvanostatical cycling tests and electrochemical impedance spectroscopy (EIS). The XRD results indicate that the phases are composed of β-Sn, Sb, Ag_3Sb, Ag_3Sn and SnSb in the $SnSbAg_x$ alloy. The existence of inactive element Ag and the complex multi-step reaction mechanism in $SnSbAg_x$ alloy anodes are propitious to improve the structure stability and thus improve the cycling performance. When cycled at a constant current density of 0.1 $mA \cdot cm^{-2}$ between 0.1 and 1.50 V, SnSbAg alloy shows better performance that the first discharge capacity is 794 $mAh \cdot g^{-1}$ and the reversible capacity of 20th cycle attains to 327 $mAh \cdot g^{-1}$. EIS results show that the semicircle relates to the passivation on the surface in the higher frequency zone and the bias relates to the diffusion in the lower frequency zone.

Keywords: Lithium-Ion Battery, Alloy Anode, $SnSbAg_x$, Reductive Co-Precipitation Method, Electrochemical Properties.

1. INTRODUCTION

With the rapid developments of the hybrid electric vehicles and portable electric devices, higher requirements have been put forward for lithium-ion batteries such as higher specific energy and larger energy density which mean abilities of charging-discharging quickly. At present, the commercial lithium-ion batteries have $LiCoO_2$ used as cathode materials, and graphite used as anode materials. The capacities of the above mentioned electrode materials are nearly to these' theoretical capacity, therefore, the developmental researches of the new electrode material are significant.[1–3]

Nowadays, the graphite is used as negative materials of the commercial lithium-ion battery. However the capacity of the graphite is lower and it has potential safety hazards, which can't already meet people's requirements. Because the single metal has higher theoretical capacity, for example, the theoretical specific capacity of Sn is 990 $mAh \cdot g^{-1}$, which aroused the attention from people. But there is greater volume expansion or shrinking for the single metal in the course of lithium-ion intercalation and dis-intercalation, then the metel anode is easily to be powders without good cycle performance. And the alloy materials can be synthesized to relieve the volume effect that the single metal produces in the course of charging and discharging. Due to the higher theoretical capacities and different voltage range of reacting with lithium for Sn and Sb, they can be prepared as the alloy anode. Sn and Sb belong to the "active" elements relative to Li, which have volume changes in the course of reversible lithium insertion, and have limit in improving the circulation performance of alloy anode. In this paper, SnSb base alloy doping with different amount of Ag are synthesized, and the effects of the inactive element Ag on the electrochemical properties of SnSb are studied.[4–6]

2. EXPERIMENTAL DETAILS

SnSbAg alloy anode powders were synthesized using chemical reductive co-precipitation method.[7] To produce the $SnSbAg_x$, the molar ratio of $SnCl_2 \cdot 2H_2O$, $SbCl_3 \cdot 2H_2O$ and $AgNO_3$ were 1:1:x ($x = 0, 0.2, 0.6, 1.0$), and the solvent was $C_6H_5Na_3O_7 \cdot 2H_2O$. They were mixed together

*Author to whom correspondence should be addressed.

 1533-4880/2010/10/7025/006 doi:10.1166/jnn.2010.2770

and dissolved in 100 ml distilled water to form a 0.1 M solution. The 0.2 M alkaline $NaBH_4$ aqueous solution (pH > 12) was added drop wise to the above mixed aqueous solution under strong magnetic stirring at room temperature. The superfluous $NaBH_4$ solution was used to ensure a complete reduction of the metal ions. After co-precipitation, all alloy powders in the aqueous solution were aged in the water bath with a constant temperature of 80 °C for 5 h. Then, the solution was filtered and the product was washed thoroughly using distilled water and acetone. The black product was dried at 105 °C for 10 h under vacuum.

The crystal structure of obtained alloy anode materials was detected by using D/Max-3A type X-ray diffraction with Cu Kα radiation ($\lambda = 1.5406$). The scanning rate and step of the half width value were 10 °C · min^{-1} and 0.02°, separately. The morphology and particle size of the alloy powders were observed by JSM-6700 type field-emission scanning electron microscopy.

Electrochemical experiments were carried out in two electrode Swagelok cells which was composed of a metallic lithium foil as counter electrode, 1 M $LiPF_6$ in ethylene carbonate (EC)–diethyl carbonate (DEC) (1:1, v/v) as electrolyte, Celegard 2400 as separator and nano-sized alloy as the working electrode. The working electrodes were prepared by pasting slurry onto a copper foil substrate. The slurry consisted of 80 wt% alloy powder, 10 wt% acetylene black and 10 wt% polyvinylidene fluoride (PVDF) dissolved in NMP. Then the electrodes were dried in vacuum oven at 100 °C for 10 h prior to use. Testing cells were assembled in an argon-filled glove box and were cycled on the Arbin BT2000 battery tester at a constant current density of 0.1 mA · cm^{-2} in the different voltage range such as 0.02–1.50 V, 0.05–1.5 V or 0.1–1.5 V. And the cycling performance software was Arbin MITS PRO multi-functional software.

The electrochemical impedance spectroscopy tests were done using tri-electrode system on the AMETEK VersaSTAT MC-4 electrochemical working station, and the reference electrode or the counter electrode was metal lithium foil, and the working electrode was made by the above mentioned method. The scanning rate was 0.1 mV · s^{-1} and the scanning voltage range was between 0 V and open voltage. The scanning frequency range were between 10^6 and 0.01 Hz. The EIS software was V3-Studio software.

3. RESULTS AND DISCUSSION

The comparisons of the XRD patterns for SnSb based alloy anode doping with different amount of Ag are shown in Figure 1. It can be seen that there are three main crystal phases existing in alloy anode materials prepared using chemical reductive co-precipitation method, which are Ag_3Sn, Ag_3Sb and SnSb. The peak intensity of the β-Sn phase diffraction of the alloy is stronger, with the decrease of Ag content. When the doping amount of Ag is 0.2, the peak intensity of the β-Sn phase diffraction of the alloy is the strongest. It caused by the Sn "excessive" due to the reduced amount of Ag_3Sn phase. It can be also found that there appears some impurity peaks with the reduced content of Ag, whose intensity are weaker. When the Ag content is 1.0, the SnSb based alloy anode with little impurity is synthesized.

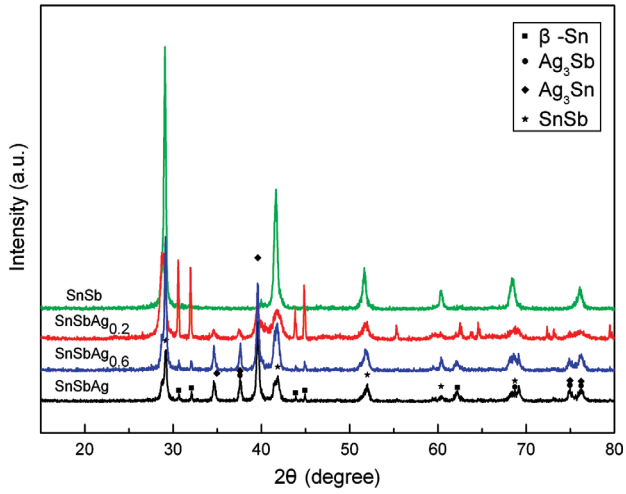

Fig. 1. The comparisons of XRD patterns for SnSb based alloy anode doping with different content of Ag.

The SEM photos of different content of Ag doped in SnSb based alloy anode are illustrated in Figure 2. The marked symbol of (a), (b), (c), (d) represents SnSb, $SnSbAg_{0.2}$, $SnSbAg_{0.6}$, SnSbAg alloy separately. In Figure 2(a), it can be observed that the particle of the SnSb alloy is bigger, which appears the form of lump in different sizes, and the average size range is between 100 nm and 400 nm. Moreover, with the increase amount of Ag, the average size of the SnSbAg alloy particle is reduced. Specially, the size of $SnSbAg_{0.6}$ is smaller than that of $SnSbAg_{0.2}$, which is nearly to that of $SnSbAg_{1.0}$.

Figure 3 is compared for the electrochemical circulation performance of SnSb base alloy of different Ag content. In Figure 3, it is obviously seen that the first discharge specific capacity is nearly to 850 mAh · g^{-1}, which is more than that of its theoretical capacity. It is due to that the SnSb occurred the irreversible reaction at the discharging voltage more than 1.0 V, which improved the first discharging capacity, but reduced the circulation performance of the alloy, then the discharge specific capacity is 258 mAh · g^{-1} after 20th cycle, which is on one-forth of the first discharge specific capacity. These actions included the decomposition of the electrolyte on the surface of the alloy, the formation of the SEI film, and the reductions of the oxidant on the surface of the SnSb alloy.[8, 9] As shown in Figure 3, with the increase of Ag content, the circulation performance of SnSb base alloy is improved. When the conten of Ag is 1.0, the discharge specific capacity of the $SnSbAg_{1.0}$ is 327 mAh · g^{-1} after 20th cycle. Moreover, as shown in Figure 1, when

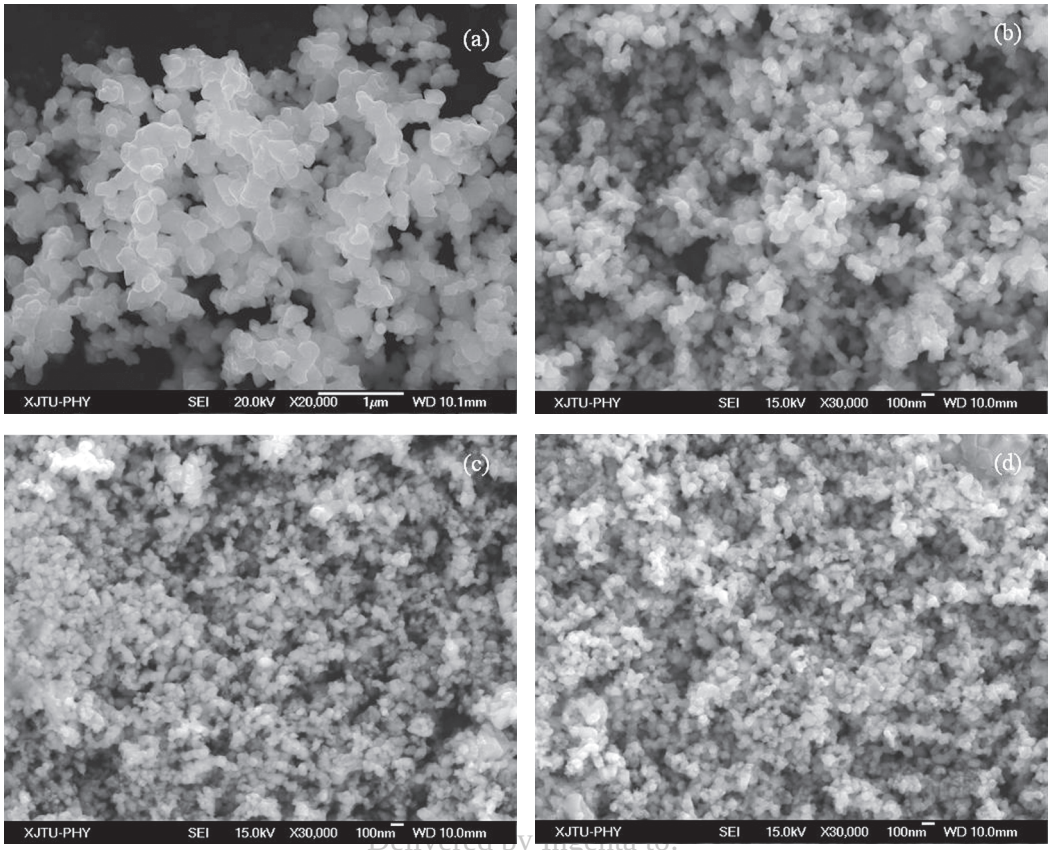

Fig. 2. The SEM photos of different content of Ag doped in SnSb based alloy anode (a) SnSb; (b) $SnSbAg_{0.2}$; (c) $SnSbAg_{0.6}$; (d) $SnSbAg_{1.0}$.

the element of Ag existed in the formation of intermetallic compounds such as inert phase, which can buffer the volume effects of Sn, Sb in the course of the Sn and Sb acting with lithium, thus improved the electrochemical circulation stability of SnSb base alloy anode. It can be easily seen in Figure 3 that the first irreversible capacity of SnSbAg alloy is much higher than that of SnSb. It is explained that the size of the alloy particle was reduced with the increase content of Ag, which is shown in Figure 2. While the size of the alloy particle is reduced, the particle has much more specific surface, and then the SEI films between the electrolyte and these surface are increased, so the first irreversible capacity is higher. When the Ag amount is nearly to 1.0, the first irreversible capacity is 350 $mAh \cdot g^{-1}$, as shown in Figure 4. So this irreversible capacity compensated the reducing capacity of doping Ag to the SnSb based alloy.

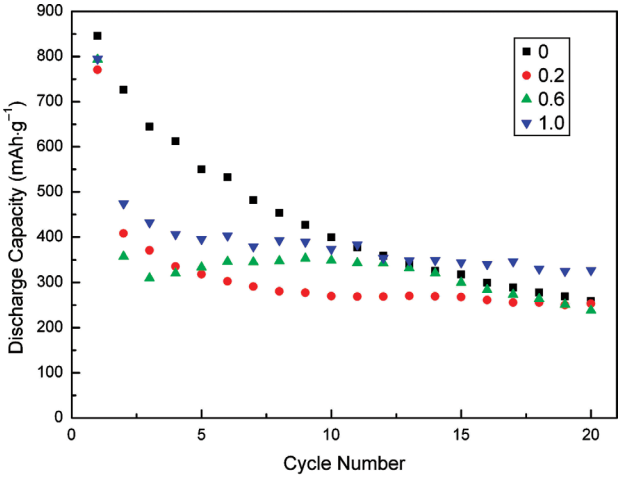

Fig. 3. The comparison of the electrochemical circulation performance of SnSb base alloy of different Ag content.

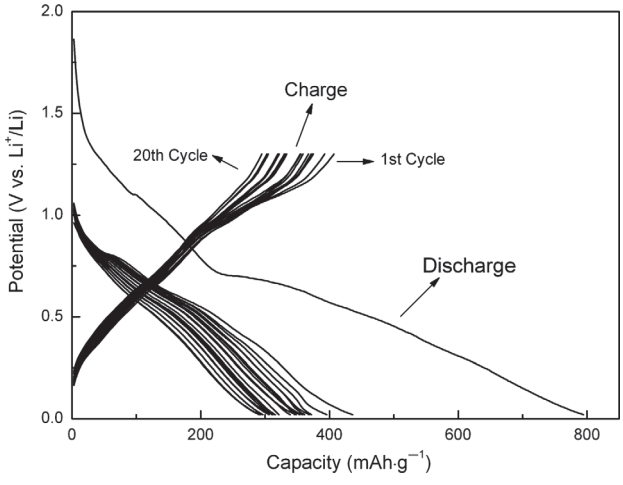

Fig. 4. The charge–discharge curves of SnSbAg.

Ag can react with lithium and turn into a series of intermetallic compounds such as Li_xAg ($x \leq 12$). However, this reaction voltage is much lower than that of Sn or Sb reacting with Li. Thus lower voltage can be used as different cutoff voltage in the course of charge–discharge cycle, which made Ag play a different role in improving the electrochemical perfornance of the alloy anode materials. The cyclic performances of SnSbAg at different cutoff voltage limit are illustrated in Figure 5. While the cutoff voltage limit is 0.02 V, the first discharge capacity of the alloy anode is nearly to 990 $mAh \cdot g^{-1}$. The first discharge capacity is gradually reduced with increasing the cutoff voltage limit. As the cutoff voltage is 0.1 V, the first discharge capacity is only 560 $mAh \cdot g^{-1}$. It is due to the reaction between Ag and Li is inhabited while the cutoff voltage limit is much lower, and Ag reacted with Li in the formation of alloying react which contributed partial capacity. When the cutoff voltage is higher, Ag could not react with Li in time, and lead to deduce of the first discharge capacity, thus means the element Ag existing in the formation of the inert phase.[10, 11] It is also can be observed that the cyclic performance drops to some extent with the lower cutoff voltage limit. It is caused that Ag react with Li, which made the main structure changing in the course of intercalation or dis-intercalation, wakening Ag to buffer the function on the volume effect of main structure.

For SnSbAg without charging–discharging, the electrochemical impedance diagram in complex plane and its fitting equivalent circuit are shown in Figure 6. It is can be observed that the impedance spectrum is made up of half arc of the high-frequency zone and oblique line of the low frequency zone, which can be presented with the equivalent circuit in the lower right of the Figure 6, while the SnSbAg alloy anode has no reaction. In the Figure 6, R_Ω represents the solution resistance of the electrode system. Q is a component of constant phase angle, which represents the difference between the frequency characteristics of the double layer capacitor of the solid electrode and that

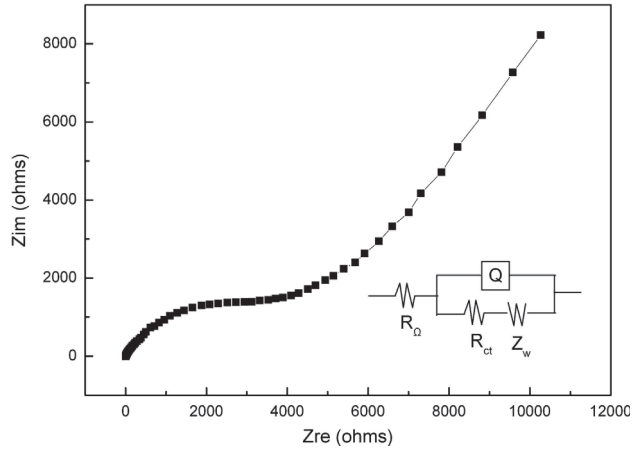

Fig. 6. For SnSbAg without charging–discharging, the electrochemical impedance diagram in complex plane and its fitting equivalent circuit.

of the "pure capacitor"; R_{ct} represents the charge transfer impedance; Z_w is the Weber impedance related to the diffusion of the Lithium ion of the alloy anode materials. Because the SnSbAg alloy anode occurs irreversible reaction to some extent in the practical electrochemical testament, the oblique line in the impedance spectrum shown in Figure 6 has a deviation from the theoretical Warburg impedance.

The database of the equivalent circuit component which carried by ZSimpWin analyzing software is used to analyze the real equivalent circuit component of the electrodes of testing battery. The electrochemical impedance diagrams in complex plane of SnSbAg when discharged to 0.2 V, as well as the fitting equivalent circuit, are shown in Figure 7. It is can be seen that the impedance spectrum is similar to Figure 6 which without charging–recharging, and also made up of a half arc in the high-frequency zone and an oblique line of $\pi/4$-like in the low frequency zone, therefore can be fitted by one equivalent circuit.

The current density can influence the charge–discharge speed directly. The cyclability comparisons of SnSbAg

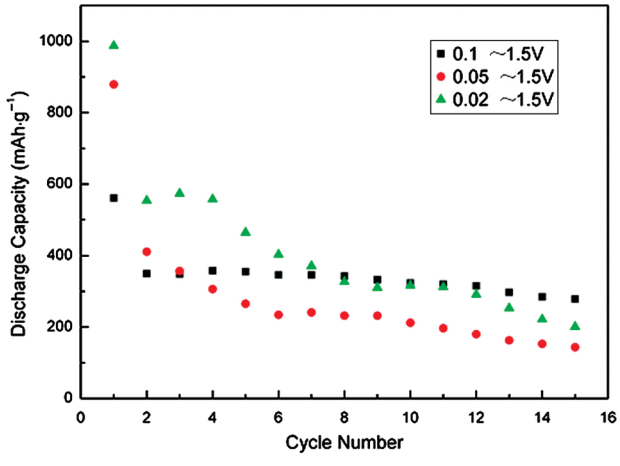

Fig. 5. The cyclic performances of SnSbAg with different cutoff voltage limit.

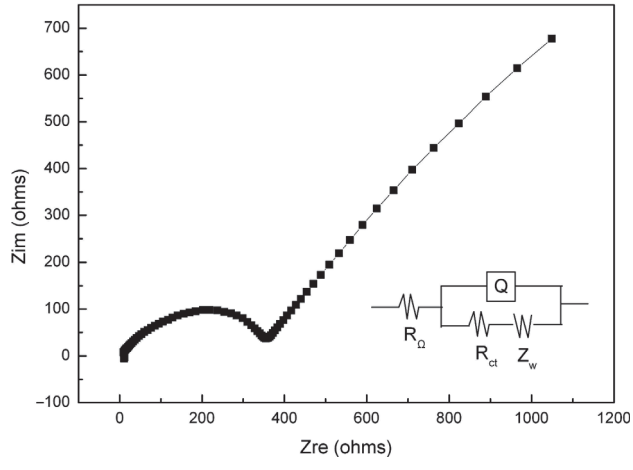

Fig. 7. The electrochemical impedance diagrams in complex plane of SnSbAg when discharged to 0.2 V, as well as the fitting equivalent circuit.

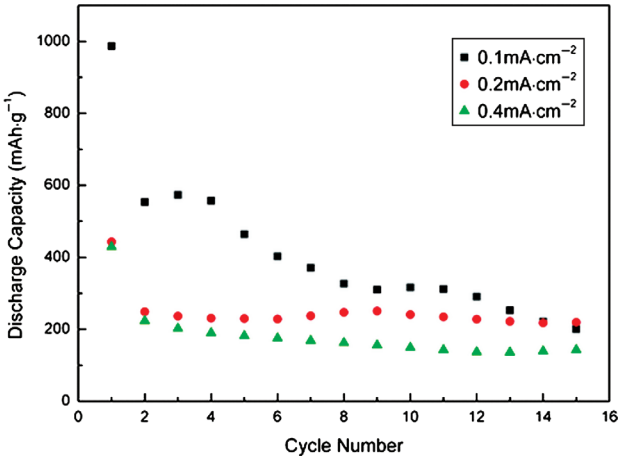

Fig. 8. The comparisons of SnSbAg cyclability at different current density.

alloy are shown in Figure 8. It can be observed that the 1st discharge capacity of the SnSbAg alloy increases with the decrease of discharge current density. When the current density is 0.1 mA · cm^{-2}, the 1st discharge capacity is about 990 mAh · g^{-1}. As the SnSbAg alloy discharged at lower current density, the electrode polarization reduced, and the phenomenon of voltage delay was weaken, then the voltage decrease of the reduction reaction was reduced, so silver can react with other metal within the voltage range. However, if the SnSbAg alloy charged at larger current density, the reaction rate was quick, and the lithium reacted with the other metal at the surface of the electrode materials, then the majority of the active materials can not react with lithium, so the amount of the intercalation lithium was little, which leads to the 1st discharge capacity reducing. For example, when the SnSbAg alloy discharged at 0.4 mA · cm^{-2}, the 1st discharge capacity was 420 mAh · g^{-1}. Simultaneously, the electrode polarization was serious, and the silver cannot react with other metal.

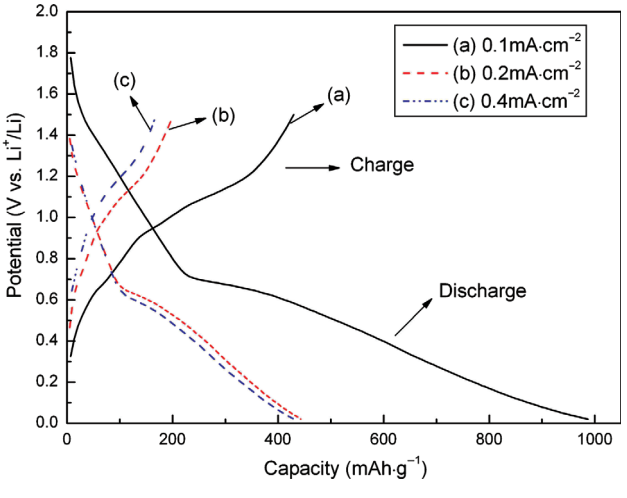

Fig. 9. The comparisons of the SnSbAg charge–discharge performance at different current density.

Figure 9 illustrates the comparasion of SnSbAg charge-discharge performance at different current density. It can be seen from the Figure 9(a) that the discharge curve appears to a long slope at current density of 0.1 mA · cm^{-2} which is corresponding to the alloy reaction of silver with lithium, and the contributing discharge capacity is 250 mAh · g^{-1} at lower discharge voltage of 0.2 V. When the current density is increased as shown in Figures 9(b and c), the voltage reaction plateau is shorten, and it is means that the voltage of the reaction plateau of Sn, Sb with Li is shorten. Then the discharge capacity is lower than 500 mAh · g^{-1} at voltage of 0.2 V. It is also can be seen that the oxidation voltage plateau rises with the increase of current density. When the SnSbAg alloy discharged at 0.4 mA · cm^{-2}, the 1st discharge capacity of SnSbAg is much lower such as about 200 mAh · g^{-1}.

4. CONCLUSION

SnSbAg alloy anode materials were synthesized using chemical reductive co-precipitation method, which appeared regular shape with small particle size. And with the increase of doping Ag amount, the particle size of the alloy anode materials decreased. The first dicharge capacity of SnSbAg is 794 mAh · g^{-1}, and the discharge capacity after 20th cycle is 327 mAh · g^{-1}. Moreover, the electrochemical performance of SnSbAg alloy anode can be improved by means of adjusting cutoff voltage limiting the reaction of Ag with Li, although the discharge capacity decreased. The electrochemical impedance spectrum of SnSbAg, when discharged to 0.2 V, is made up of a half arc in the high-frequency zone and an oblique line of $\pi/4$-like in the low frequency zone, which is similar to that of SnSbAg without charging–discharging. Meanwhile, the two parts of the impedance spectrum also represent impedance responds of the electrode surface passivation layer and mass transfer respectively. Furthermore, going with the charge–discharge reaction, the charge transmission impedance R_{ct} deduced and the Warburg impedance Z_w increased.

Acknowledgment: The authors would like to acknowledge Xi'an Applied Materials Innovation Fund Application (XA-AM-2008-16), Xi'an Jiaotong University Inter-disciplinary Project Fund (0109-08140020), and Xi'an Jiaotong University Graduate Student Innovates Fund for providing financial support to this work.

References and Notes

1. L. Y. Beaulieu, K. C. Hewitt, J. R. Dahn, R. L. Turner, A. Bonakdarpour, A. A. Abdo, L. Christensen, K. W. Eberman, and L. J. Krause, *J. Electrochem. Soc.* 150, A149 (**2003**).
2. L. Hong, H. Jin, and H. Xuejie, *Solid State Ionics, Diffusion and Reactions* 178, 265 (**2007**).

3. I. Grigoriants, A. Soffer, G. Salitra, and D. Aurbach, *J. Power Sources* 146, 185 **(2005)**.
4. F. Wang, M. S. Zhao, and X. P. Song, *J. Alloys Compd.* 439, 249 **(2007)**.
5. S. S. Zhang, K. Xu, and T. R. Jow, *Electrochim. Acta* 51, 1636 **(2006)**.
6. A. Sivashanmugam, T. Prem Kumar, N. G. Renganathan, S. Gopukumar, M. Wohlfahrt-Mehrens, and J. Garche, *J. Power Sources* 144, 197 **(2005)**.
7. F. Wang, M. S. Zhao, and X. P. Song, *J. Alloys and Compd.* 472, 55 **(2009)**.
8. S. Naille, C. M. Ionica-Bousquet, F. Robert, F. Morato, P.-E. Lippens, and J. Olivier-Fourcade, *J. Power Sources* 174, 1091 **(2007)**.
9. M. Stjerndahl, H. Bryngelsson, T. Gustafsson, J. T. Vaughey, M. M. Thackeray, and K. Edström, *Electrochim. Acta* 52, 4947 **(2007)**.
10. F. Wang, M. S. Zhao, and X. P. Song, *J. Power Sources* 175, 558 **(2008)**.
11. L. Simonin, U. Lafont, and E. M. Kelder, *J. Power Sources* 180, 859 **(2008)**.

Received: 4 September 2009. Accepted: 30 October 2009.